Nano Today 38 (2021) 101152

Contents lists available at ScienceDirect

Nano Today

journal homepage: www.elsevier.com/locate/nanotoday

Machine-learning micropattern manufacturing

Si Wang[a], Ziao Shen[a], Zhenyu Shen[a], Yuanjun Dong[a], Yanran Li[a], Yuxin Cao[a], Yanmei Zhang[b], Shengshi Guo[a], Jianwei Shuai[a], Yun Yang[a], Changjian Lin[b], Xun Chen[c,*], Xingcai Zhang[d,e,**], Qiaoling Huang[a,***]

[a] Research Institute for Biomimetics and Soft Matter, Fujian Provincial Key Laboratory for Soft Functional Materials Research, Department of Physics, College of Physical Science and Technology, Xiamen University, Xiamen 361005, China
[b] State Key Laboratory for Physical Chemistry of Solid Surfaces, and Department of Chemistry, College of Chemistry and Chemical Engineering, Xiamen University, Xiamen 361005, China
[c] Wenzhou Institute, University of Chinese Academy of Sciences, Wenzhou 325000, China
[d] John A. Paulson School of Engineering and Applied Sciences, Harvard University, Cambridge, MA 02138, United States
[e] School of Engineering, Massachusetts Institute of Technology, Cambridge, MA 02139, United States

ARTICLE INFO

Article history:
Received 13 September 2020
Received in revised form 8 March 2021
Accepted 4 April 2021
Available online xxxx

Keywords:
Machine learning
Micropattern manufacturing
Decision tree (DT) modeling
Gradient boosted regression tree (GBRT) modeling
Bipolar electrochemistry manufacturing
Materials screening

ABSTRACT

Micropatterning has been widely applied in electronics, biomaterials engineering, and microfluidics studies. A key challenge in using bipolar electrochemistry for fabricating titanium dioxide (TiO_2) nanotube micropatterns (TNMs) with desired properties is to balance interrelated experimental parameters and define experimental boundary conditions. For example, it is challenging to determine the anodization voltage boundary as high anodization voltage with certain conditions might induce titanium foils rupture. Here, we utilize active learning to facilitate the optimization process of fabricating TNMs with a wide dimension range within one sample using bipolar electrochemistry. Starting with a small dataset, the decision tree model differentiates normal data from abnormal data (i.e., titanium foils ruptured), which helps define the experimental boundaries. Then gradient boosted regression tree (GBRT) model analyzes the data and provides predictions and directions for optimizing TNMs. Then predictions are verified by experiments, and new results update the training dataset for the next learning loop. Results show that ML algorithms well define the experimental boundary conditions. And only within several iterations, we obtained the optimal TNMs with a diameter range of 27–470 nm, expanding the gradient to the largest extend without tedious experiments. Those results indicate that machine learning algorithms are effective in accelerating materials manufacture and optimization. Further silver nanoparticle doping demonstrates that large-scale TNMs are effective platforms for high-throughput screening.

Introduction

Design/fabricate biomaterials with desirable functions for specific applications is a critical goal in biomedical research. The inherent complexities in the structure-property-function relationships of biomaterials raise the challenge of designing and fabricating biomaterials. Notably, the traditional evaluation process requires multiple samples for evaluation, which is tedious and cumbersome. Herein, optimizing biomaterials with desirable properties by fewer experiments and materials becomes an essential and urgent task in materials genome initiative [1–3].

Micropatterning techniques miniaturize and integrate various materials with different properties into platforms that are useful for high-throughput screening of biomaterials with fewer samples and high efficiency [4,5]. Popular micropatterning techniques include soft lithography, photolithography, jet patterning, scanning-probe lithography, laser-guided patterning, microfluidics, bipolar electrochemistry, etc. [6–9] Many of those techniques usually involve complicated multi-steps. For example, the photolithography approach consists of photoresist coating, exposure, development, and etching [10].

Among all micropatterning techniques, bipolar electrochemistry is a simple one-step method and has been widely utilized for

* Corresponding author.
** Corresponding author at: John A. Paulson School of Engineering and Applied Sciences, Harvard University, Cambridge, MA 02138, United States.
*** Corresponding author.
E-mail addresses: chenxun@ucas.edu.cn (X. Chen), xingcai@mit.edu (X. Zhang), qlhuang@xmu.edu.cn (Q. Huang).

https://doi.org/10.1016/j.nantod.2021.101152
1748-0132/

constructing chemical/structure gradient micropatterns [11–14], including silver micropatterns [14], gold micropatterns [15], copper micropatterns [16], etc. As titanium dioxide (TiO_2) nanotubes (TNs) have been broadly developed and applied in many fields (such as biomedical applications, sensing, photocatalysis, etc.), some research groups are devoted to constructing TiO_2 nanotube micropatterns (TNMs) using bipolar electrochemistry for high-throughput applications [17–19]. By tuning parameters of bipolar electrochemistry (e.g., electrolyte type, concentration, voltage, time, etc.), Loget et al. obtained TNMs with a diameter range of 200 nm and utilized them for photocurrent screening [20]. However, it has been reported that the diameter of TNMs from the conventional anodization method could be as large as ~750 nm [21]. The remaining question is that could we find the optimal TNMs with the widest diameter range for thorough high-throughput studying?

Unfortunately, we found it challenging to achieve this goal by traditional statistical methods because of the enormous complexity of bipolar electrochemistry. By fixing the electrode cell (the size of bipolar electrode, electrolyte volume, and the distance between bipolar electrode), we previously obtained TiO_2 nanotube micropatterns (TNMs) with a diameter range of 20–350 nm [22]. We found that even though higher applied voltage could enlarge nanotube diameter, it might accelerate the current and ruptures the titanium foil during anodization. But a slight change of other parameters (temperature, stirring speed, electrolyte concentration, water volume) might save the foil from break. So we certainly could obtain TNMs with a wider diameter range after enormous experiments; however, we will always wonder will the diameter range be wider if we carry out more tests. Herein, we need other methodology to define the optimal gradient or the experimental boundaries to avoid the rupture of titanium foils that we can navigate the optimal path by least experiments.

As a particular case of machine learning, active learning (AL) actively chooses the data samples on which it wants to learn from and addresses the issue of large dataset labelling [23]. Supervised machine learning models usually require a large training dataset to achieve satisfactory accuracy. However, labeling a large dataset is expensive and time-consuming, or even need to be accomplished by a human expert of a specific domain. With active learning, we only need to label the most informative subset of the whole dataset. Active learning takes an iterative process to improve the accuracy of the model; it trains the model on an initial data subset and queries more data labeling in the next round according to the evaluation results in this round. So it has been widely applied in many research areas [23,24]. For example, Yuan et al. expedited the discovery of new Barium titanate ($BaTiO_3$) based piezoelectrics with large electrostrains with the aid of active learning [25].

Herein, active learning might be a great tool to solve the aforementioned difficulties in optimizing large-scaled gradient TiO_2 nanotube micropatterns (TNMs) with a wider diameter range. In this paper, we apply machine learning methods to confine the experimental boundary conditions of bipolar electrochemistry and expedite the optimization of fabricating TNMs by active learning. Through several active learning iterations, we obtain the optimal TNMs (with a diameter range of 27–470 nm) using the least experiments. Further silver nanoparticles (AgNPs) doping was applied as a case study for high-throughput studying.

Results and discussion

Optimizing TiO_2 nanotube micropatterns with active learning

Fig. 1 illustrates the active learning loop, which shows the learning methodology to lead bipolar electrochemistry experiments to optimize TNMs. To initiate the machine learning iteration, we collect both experimental parameters (features) and results (maximum diameter of each TNM) from the fabrication process. After data collection, the initial data (training data) are imported for active learning. Machine learning algorithms study/analyze/classify the pattern of training data and build prediction models. Experiments

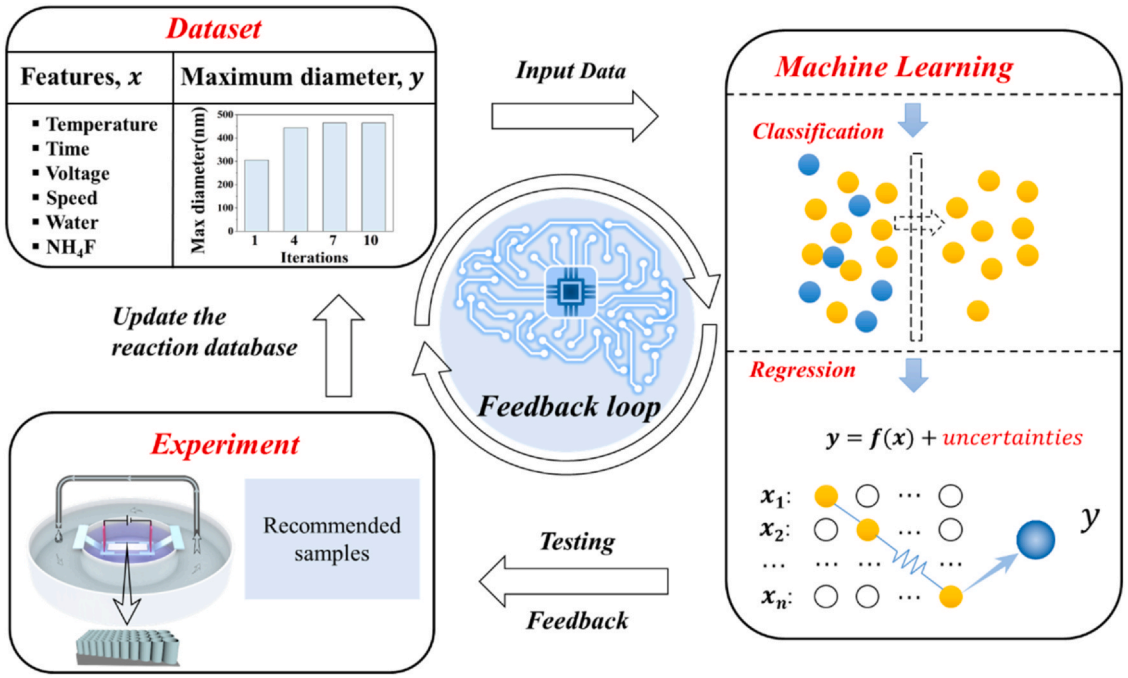

Fig. 1. An overview of active learning iteration for accelerating optimization process of TiO_2 nanotube micropatterns (TNMs). The relationships between the maximum diameter (y) of TNMs on gradient sample and experimental parameters x (i.e., temperature, time, voltage, stirring speed, water volume, electrolyte concentration) are analyzed by machine learning algorithms, which further predict optimal parameters for testing. For the experimental features, temperature represents the temperature of the circulating water, time stands for the anodization time for fabricating TNMs, voltage represents the applied anodization voltage, speed means the stirring speed of the magnetic stirring bar, water and NH_4F represent the water volume and the mass fraction of NH_4F in the electrolyte.

validate predicted data, and new results further update the training dataset for the next learning loop. By looping machine learning and experimental validation, we can maximize the diameter range of TNMs by the least experiments.

The first step of the active learning iteration is to perform bipolar anodization experiments. It is well known that nanotube diameter increases with applied voltage. So at the beginning we focused on escalating applied voltage. Sometimes, during the anodization process, titanium foils rupture from the middle when the anodization current rises too high. We found that even though higher applied voltage could enlarge nanotube diameter, it might accelerate the current and ruptures the titanium foil during anodization (pink areas in Fig. S1a). Then there are no measurable results for the maximum diameter of TNMs. But this information is precious as it indicates that there is a experimental boundary. Herein, we collect not only valid data with measurable maximum nanotube diameter, but also "unwanted" data without measurable nanotube diameter (hereafter identified as "cut-off" points).

There are more than twenty popular learning algorithms in machine learning algorithms [26–29]. To differentiate cut-off points from the standard dataset, we compared several suitable classification algorithms, including K-Nearest Neighbor (KNN) [30], Bayes [31], Support Vector Machine (SVM) [32], Decision tree (DT) [1], Gradient Boosting Decision Tree (GBDT) [33] (Section S4 in the electronic supplementary information, ESI†). As shown in Fig. S2a, both DT and GBDT have higher accuracy than other methods. However, compare the learning curves of GBDT to that of DT (compare Fig. S2b and c), GBDT has a large gap between training and cross-validation curve, indicating slight overfitting of the GBDT model. Therefore, the decision tree is adopted as a classifier to classify cut-off points from the typical dataset as shown in Fig. S3. Fig. 2a shows the correlation of experimental features after dimension reduction with the t-distributed stochastic neighbor embedding (t-SNE) method in the Scikit-learn library (Section S1.4 in the ESI†) [34]. The clear boundary between valid experimental features (black dots) and cut-off points (red dots) illuminates the success of classification. More importantly, this boundary sets the boundaries for the regression model, i.e., it helps define experimental boundaries of each feature in fabricating a typical TNM without sample rupture.

As the classification builds the experimental boundaries, only valid data are imported as a training dataset for further regression. We need another machine learning algorithm to generate a "model" from the data, that is, a "regression algorithm". Among all, we only present six representative algorithms based on the logic of "linear model, nonlinear model, integrated model and neural network", including linear regression [35], polynomial regression [36], support vector regression (SVR) [37], decision tree (DT), gradient boosted regression tree (GBRT) [38], and neural network (NN) [39,40] (Section S5 in the ESI†).

A statistical inference model $y = f(x) +$ uncertainties is trained to predict the maximum diameter y of the nanotubes on the TNMs from experimental features x, where f represents learned relationships between y and x. The uncertainties are associated with the model fitting, such as mean absolute error (MAE) and coefficient of determination (R^2), which will be addressed in detail later. Among all six regression models, the neural network is a powerful tool in many fields, including computer vision. However, we found that it may not be the most suitable model for small datasets (ESI† Figs. S4 and S5). On the contrary, the GBRT model presents best in estimating f with the least errors and it is further employed for prediction and optimization.

Fig. 2b compares the experimental results (maximum diameter of TNMs characterized from scanning electron microscope images) to the predictions from the empirical value ("exploration data", obtained from linear regression of experimental results) and machine learning. Seven different test conditions are randomly chosen from our dataset for comparison. Apparently, the empirical prediction is far from satisfactory, whereas prediction from the machine learning algorithm has a better fit with experimental results.

Fig. 3a shows the maximum diameter of TNMs obtained by experiments and machine learning prediction from each iteration. Apparently, at the beginning of the loop, the actual test value is distinct from prediction. The poor prediction at the beginning is understandable as the dataset is small. It has been widely approved that, with a large dataset, machine learning can precisely predict material property under certain conditions [41]. If we only need to predict material property, traditional machine learning is a perfect tool for prediction when sufficient data is collected. But this is not the optimal strategy in our case as we are aiming at optimizing TNMs by fewer experiments (i.e., higher efficiency). Thus, we start applying the GBRT methodology with a small amount of data and predicting the potential optimal parameters. Therefore, it is inevitable that the accuracy of the initial fitted model is low with high bias or uncertainty. Given the circumstance, the performance of the

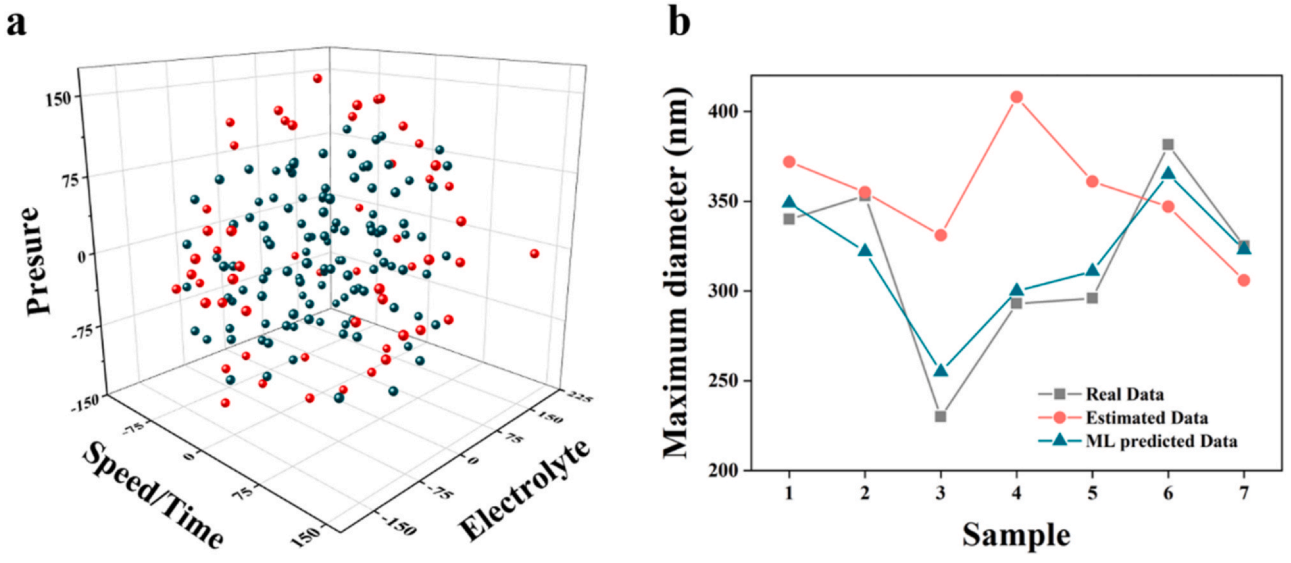

Fig. 2. (a) Diagram shows effective experimental features surrounded by cut-off points. (b) Experimental comparisons of exploration data and machine learning data showing that machine learning can provide more reliable guidance.

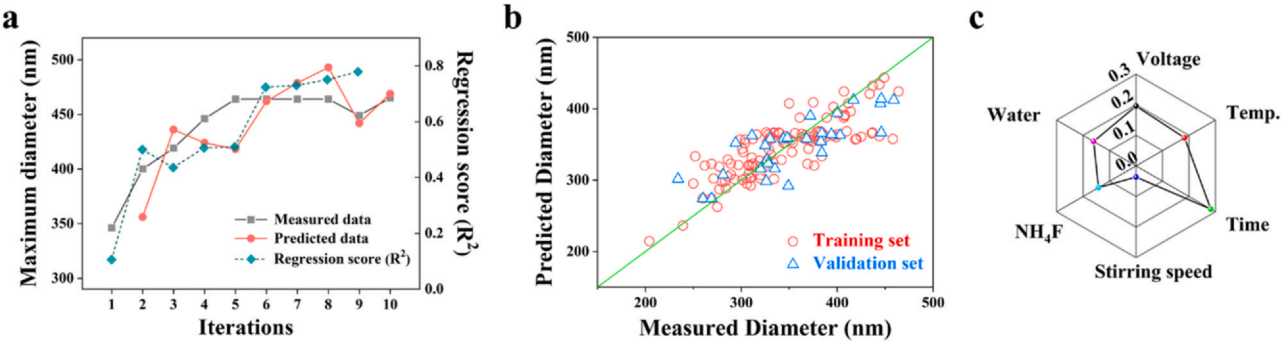

Fig. 3. (a) Effects of validation data on ML models for the maximum diameter (of TNMs), which converges as iteration increases. R^2 represents that the performance of the GBRT model increases with the iteration number. (b) A comparison between the predicted and the measured maximum diameter of TNMs validates the GBRT model. (c) The importance of each experimental feature in GBRT.

GBRT model is not ideal with low regression score R^2 (Fig. 3a) at the beginning. Then we carry out experiments and update the training dataset iteratively. After each training loop, the collected new data replenish the training data for a better regression and design (Fig. 1). And with more data updated in each iteration, the R^2 value of the GBRT model increases to 0.78, which is apparently no perfect for the machine learning algorithm. But giving our dataset is small (only 158 samples for the GBRT model in the last loop, ESI†), the increment of R^2 with the growing amount of training data proves that the GBRT model's accuracy can be improved with the increasing amount of training data. More importantly, with the help of active learning, the tested maximum diameter of TNMs from each iteration escalates with forecast until it reaches the plateau (~470 nm) after five learning loops. This is about a 34% increase compared to the beginning value of ~350 nm. As the maximum diameter has reached a plateau, we did not keep carrying out more experiments. It is worth mention that even though we might obtain this optimal TNM after enormous experiments, we will not be able to confirm the obtained result is optimal owing to the complexity of bipolar chemistry. But with the classification model, which builds up experimental boundaries for each feature, we can affirm the extreme value is the optimal value.

The scatter diagram in Fig. 3b compares the prediction results and actual measurements. All data points scatter around the diagonal, indicating high consistency between prediction results and actual measurements. Moreover, it also suggests that our model does not overfit the data. And the concurrence between prediction and result is reasonable. The illustration obtained by GBRT in Fig. 3c represents the importance of each experimental feature. Apparently, time is one of the essential features as nanotubes' formation requires a certain amount of time. But it is unnecessary to prolong reaction time over 5 h as the nanotube diameter reaches a plateau after 5 h (ESI† Fig. S6). It seems as if stirring speed has the least effect (feature importance is 3.65%) on the maximum nanotube diameter of TNMs. But it is crucial to the formation of TNMs. Under certain conditions, increasing stirring speed will lower the reaction current. A low stirring rate may cause high current flow because the solution dissipates too slowly, and the temperature escalates. With the anodization current boosting, titanium foil consumes fast and eventually ruptures. On the contrary, when the stirring speed is too high, the stirring bar starts floating without stirring the electrolyte that the current boosts instantaneously and breaks the foil.

Table S2(ESI†) compares the optimal experimental conditions from the initial and final loop. The optimal anodization is only 160 V, which is much lower than our expectation. Based on our previous researches and publications from the literature, nanotube diameter usually increases with anodization voltage within a certain range. Therefore, at the beginning of the learning loop, we expected the optimal anodization voltage to be higher than 200 V that we focused on increasing the applied voltage and avoiding destroying the titanium foils at the same time. But the optimization results demonstrate that we need to compromise anodization voltage with other parameters to obtain a wider gradient. It also shows that machine learning algorithms can efficiently analyze electrochemistry data, build experimental boundaries, and optimize materials manufacture.

Characterization of optimal gradient TiO_2 nanotubes

Typical SEM images in Fig. 4a and S7a show self-organized nanotubes integrated within one gradient sample which is obtained from the optimal parameters of bipolar anodization. The outer diameter of TNMs boosts from ~27 to 470 nm (Fig. S7b) with nanotube length rises from 0.17 to 3.28 μm, and the nanotube wall thickens from ~5 to 22 nm (Fig. S7c), indicating the formation of gradient TiO_2 nanotubes with a wide diameter range.

Application of TNMs for high-throughput study of Ag doping

TiO_2 nanotubes have been numerously employed as a platform/vehicle for drug delivery, metal doping, and sensing. However, not much is known about how nanotube diameter affects the surface modification processes (e.g., silver doping, drug immobilization) owing to the diversity of TNs. Here, we apply optimal TNMs for a high-throughput case study of how nanotube diameter affects silver nanoparticles (AgNPs) doping (Fig. 4b) and the corresponding bacterial (Fig. 4c and d) and cell (Fig. 5) responses. We choose silver nanoparticle doping and its antibacterial application as a case study as it is a facile, easily visible, and verifiable method and we have strong expertise in this antibacterial field [14,42–46]. It is a good proof-of-concept demonstration of the machine learning algorithms as an effective method for accelerating materials manufacture, optimization, and high-throughput screening, paving the way for its broad applications. AgNPs are doped by electrochemical deposition and the high-resolution X-ray photoelectron spectroscopy (XPS) spectra presented in Fig. S8(ESI†) verified the existence of the metallic form of doped AgNPs. Fig. 4b shows that the doping process retains the nanotubular structure of TNMs. The size and the amount of AgNPs increase with the growth of nanotube diameter, suggesting large-size nanotubes are more active in silver doping than small-size nanotubes. Besides, the doping is not even as more particles distribute at the top of the nanotubes. But some nanoparticles could be found within the nanotubes' interior surfaces, indicating the silver nanoparticles can deposit at any active spot.

Fig. 4c and d represent biofilm formation after four hours culture of Gram-positive *S. aureus* and Gram-negative *E. coli* bacteria. A similar attachment pattern could be found for those two bacteria. A lot of aggregated *S. aureus* (Fig. 4c) and *E. Coli* (Fig. 4d) bacteria anchor

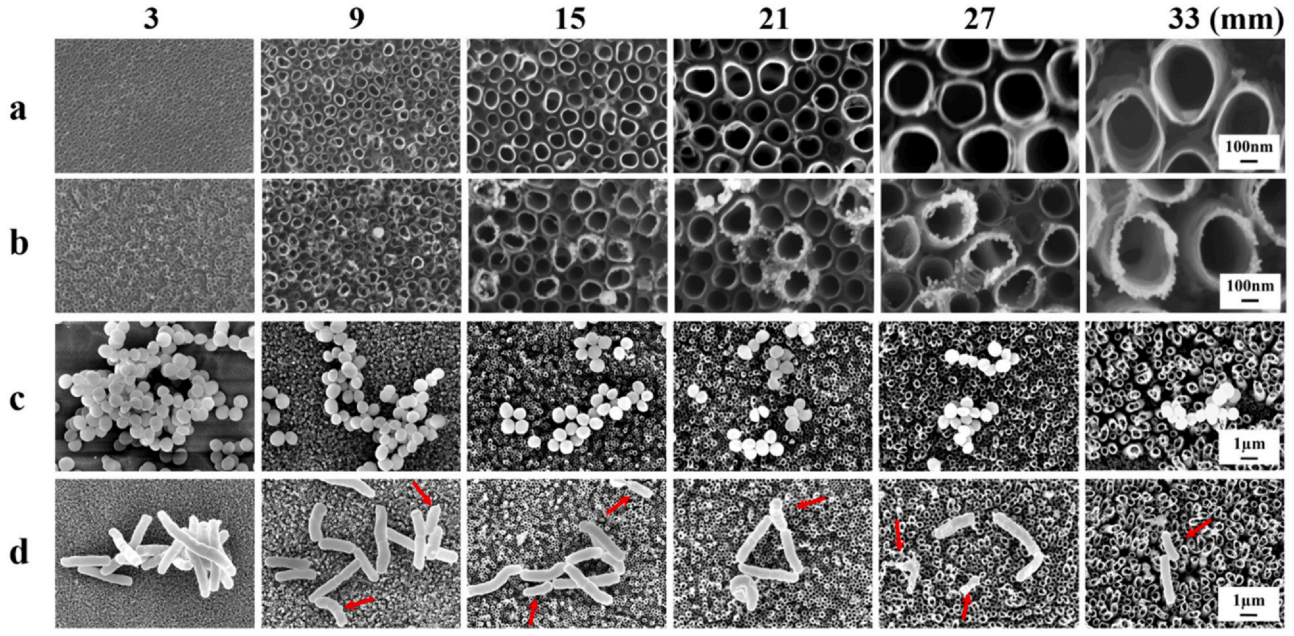

Fig. 4. (a) Top SEM images of opened TiO_2 nanotubes captured from different locations on a single gradient sample, starting from the cathode edge to the anode edge of the TNMs. (b) SEM images of deposited silver nanoparticles captured at different positions on TNMs. (c, d) Typical SEM morphologies of attached *S. aureus* cells and *E. coli* cells on the silver nanoparticle deposited TNMs (4 h).

on the small-size nanotubes. With the increment of nanotube size, the number of attached bacteria dramatically reduces that the number of adherent bacteria on the largest nanotubes has been highly suppressed, implying antibacterial property increases with nanotube diameter. Most of the adherent *S. aureus* cells are spherical and there is no significant difference in the morphology of adherent

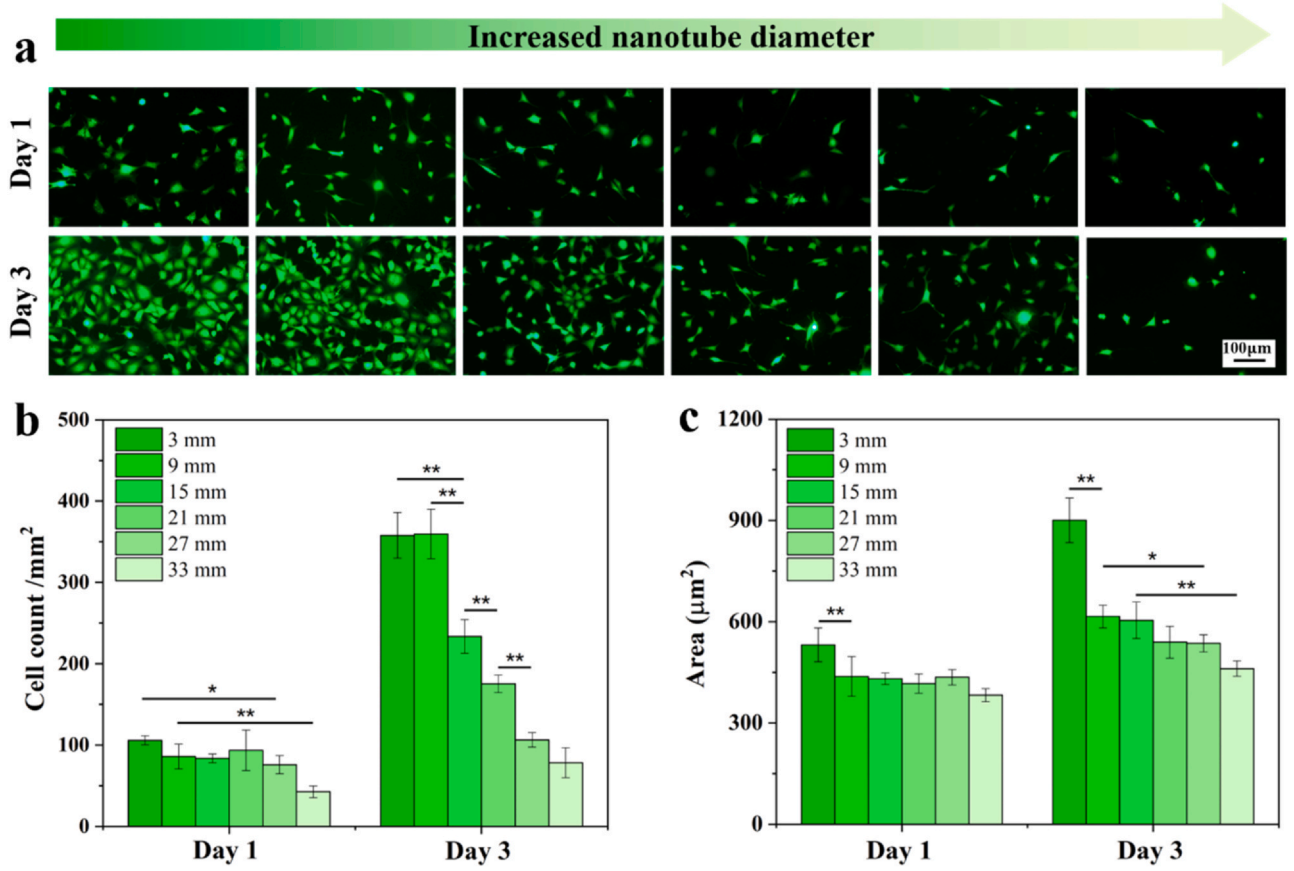

Fig. 5. Fluorescence images (a) and statistic results (b, c) of MC3T3-E1 cells on silver gradients after 1-day and 3-day culture. *$p < 0.05$ and **$p < 0.01$ indicates the significant difference.

cells across the gradient. Likewise, most adherent *E. coli* cells maintain their rod-like shape. However, some ruptured morphologies (indicated by red arrows) could be observed, suggesting AgNPs can kill bacteria through membrane rupture [14].

We further investigate MC3T3-E1 cell adhesion and proliferation on the silver gradient. On day 1, attached cell number and cell size are highest on the smallest TNs region (3 mm: 106 ± 5.5 cells/mm^2) and lowest on the largest TNs region (33 mm: 42 ± 7.3 cells/mm^2), whereas there is no noticeable difference among TNs in the middle area of the gradient. After 3 days of culture, cell density boosts across the entire silver gradient compared to day 1. On the smallest TNs region, cell density escalates from 106 ± 5.5 cells/mm^2 on day 1 to 357.7 ± 28.1 cells/mm^2 on day 3 without full confluence. The attached cells in this region of the gradient display better spread morphology, with the spreading area enlarges from 531 ± 50.1 μm^2/cell on day 1 to 900 ± 66.0 μm^2/cell on day 3. Cell density and size decrease with the increment of nanotube dimension that even though cell number at the largest TNs region increases from 382 ± 19.4 μm^2/cell on day 1 to 461 ± 22.5 μm^2/cell on day 3, the proliferation rate is much lower compared to that of small-size TNs. Overall, TNMs present a promising platform for high-throughput studying of TiO_2 nanotube-based materials.

Conclusion

In summary, we apply the active learning methodology to assist the optimal process of fabricating TNMs with a wide gradient. Results show that the DT model is well suited for the classification task to separate the cut-off points from valid data, building up the experimental boundary conditions. GBRT model learns the data pattern and further guides innovative design and fabrication. With the help of active learning, only within several learning loops, we obtain the optimal TNMs with the widest gradient of 27–470 nm. High-throughput studying of silver gradient proves that TNMs are practical platforms for high-throughput screening/study of TiO_2 nanotube-based materials. Herein, our results illustrate that machine learning algorithms provide an optimal criterion for guiding experiments in materials design/optimization. The optimal TNMs could be further utilized for thigh-throughput studying in biomedical devices, drug delivery, metal doping, photocurrent screening, corrosion resistance, photovoltaic cells, sensors, photoelectrochemical water splitting, and microfluidics fields.

It should be noted that, as machine learning models' accuracy relies on data, a certain amount of data will be required to achieve acceptable model accuracy, i.e., the optimization process is either tedious or has low model accuracy. To avoid tedious experiments throughout the learning process, the empirical, experimental designs from the beginning are crucial as the experimental data steer the model accuracy. Thereafter, a combination of a comprehensive understanding of the material fabrication mechanisms and appropriate machine learning algorithms can provide an efficient route for materials development.

CRediT authorship contribution statement

Si Wang: Investigation, Visualization, Writing - original draft. **Ziao Shen:** Investigation. **Zhenyu Shen:** Investigation. **Yuanjun Dong:** Investigation. **Yanran Li:** Investigation. **Yuxin Cao:** Investigation. **Yanmei Zhang:** Investigation. **Jianwei Shuai:** Funding acquisition, Discussion and resources. **Yun Yang:** Methodology, Writing - review & editing. **Shengshi Guo:** Methodology, Technique support. **Yun Yang:** Methodology, Writing - review & editing, Technique support. **Changjian Lin:** Resources. **Xun Chen:** Conceptualization, Supervision, Discussion, Writing - review & editing. **Xingcai Zhang:** Supervision, Discussion, Writing - review & editing. **Qiaoling Huang:** Conceptualization, Supervision, Visualization, Writing - review & editing.

Declaration of Competing Interest

The authors declare that they have no known competing financial interests or personal relationships that could have appeared to influence the work reported in this paper.

Acknowledgment

The authors would like to acknowledge the funding assistant provided by the State Key Project of Research and Development (2016YFC1100300), National Natural Science Foundation of China (11904301, 11874310, 21773199) and 111 Project (B16029).

Appendix A. Supporting information

Supplementary data associated with this article can be found in the online version at doi:10.1016/j.nantod.2021.101152.

References

[1] P. Raccuglia, K.C. Elbert, P.D.F. Adler, C. Falk, M.B. Wenny, A. Mollo, M. Zeller, S.A. Friedler, J. Schrier, A.J. Norquist, Machine-learning-assisted materials discovery using failed experiments, Nature 533 (2016) 73–76, https://doi.org/10.1038/nature17439
[2] D. Xue, P.V. Balachandran, J. Hogden, J. Theiler, D. Xue, T. Lookman, Accelerated search for materials with targeted properties by adaptive design, Nat. Commun. 7 (2016) 11241, https://doi.org/10.1038/ncomms11241
[3] T. Lookman, P.V. Balachandran, D. Xue, J. Hogden, J. Theiler, Statistical inference and adaptive design for materials discovery, Curr. Opin. Solid State Mater. Sci. 21 (2017) 121–128, https://doi.org/10.1016/j.cossms.2016.10.002
[4] L. Liu, N. Xiang, Z. Ni, X. Huang, J. Zheng, Y. Wang, X. Zhang, Step emulsification: high-throughput production of monodisperse droplets, Biotechniques 68 (2020) 114–116, https://doi.org/10.2144/btn-2019-0134
[5] M. Benz, M.R. Molla, A. Böser, A. Rosenfeld, P.A. Levkin, Marrying chemistry with biology by combining on-chip solution-based combinatorial synthesis and cellular screening, Nat. Commun. 10 (2019) 2879, https://doi.org/10.1038/s41467-019-10685-0
[6] M.S. Chowdhury, W. Zheng, S. Kumari, J. Heyman, X. Zhang, P. Dey, D. Weitz, R. Haag, Dendronized fluorosurfactant for highly stable water-in-fluorinated oil emulsions with minimal inter-droplet transfer of small molecules, Nat. Commun. 10 (2019) 4546, https://doi.org/10.1038/s41467-019-12462-5
[7] Z. Tang, N. Kong, X. Zhang, Y. Liu, P. Hu, S. Mou, P. Liljeström, J. Shi, W. Tan, J.S. Kim, Y. Cao, R. Langer, K.W. Leong, O.C. Farokhzad, W. Tao, A materials-science perspective on tackling COVID-19, Nat. Rev. Mater. 5 (2020) 847–860, https://doi.org/10.1038/s41578-020-00247-y
[8] Q. Zhang, X. Zhang, X. Zhang, L. Jiang, J. Yin, P. Zhang, S. Han, Y. Wang, G. Zheng, A feedback-controlling digital microfluidic fluorimetric sensor device for simple and rapid detection of mercury (II) in costal seawater, Mar. Pollut. Bull. 144 (2019) 20–27, https://doi.org/10.1016/j.marpolbul.2019.04.063
[9] Y. Wang, L. Lu, G. Zheng, X. Zhang, Microenvironment-controlled micropatterned microfluidic model (MMMM) for biomimetic in situ studies, ACS Nano 14 (2020) 9861–9872, https://doi.org/10.1021/acsnano.0c02701
[10] B. Jeong, H. Han, C. Park, Micro- and nanopatterning of halide perovskites where crystal engineering for emerging photoelectronics meets integrated device array technology, Adv. Mater. 32 (2020) 2000597, https://doi.org/10.1002/adma.202000597
[11] Y. Koizumi, H. Nishiyama, I. Tomita, S. Inagi, Templated bipolar electrolysis for fabrication of robust Co and Pt nanorods, Chem. Commun. 54 (2018) 10475–10478, https://doi.org/10.1039/c8cc05986a
[12] R. Gao, Y.-L. Ying, Y.-J. Li, Y.-X. Hu, R.-J. Yu, Y. Lin, Y.-T. Long, A 30 nm nanopore electrode: facile fabrication and direct insights into the intrinsic feature of single nanoparticle collisions, Angew. Chem. Int. Ed. 57 (2018) 1011–1015, https://doi.org/10.1002/anie.201710201
[13] N. Patterson, A. Ignaszak, Modification of glassy carbon with polypyrrole through an aminophenyl linker to create supercapacitive materials using bipolar electrochemistry, Electrochem. Commun. 93 (2018) 10–14, https://doi.org/10.1016/j.elecom.2018.05.021
[14] Y. Li, Y. Dong, Y. Yang, P. Yu, Y. Zhang, J. Hu, T. Li, X. Zhang, X. Liu, Q. Xu, Q. Huang, C. Lin, Rational design of silver gradient for studying size effect of silver nanoparticles on contact killing, ACS Biomater. Sci. Eng. 5 (2019) 425–431, https://doi.org/10.1021/acsbiomaterials.8b01282
[15] A. Lundgren, S. Munktell, M. Lacey, M. Berglin, F. Björefors, Formation of gold nanoparticle size and density gradients via bipolar electrochemistry, ChemElectroChem 3 (2016) 378–382, https://doi.org/10.1002/celc.201500413
[16] H. Termebaf, M. Shayan, A. Kiani, Two-step bipolar electrochemistry: generation of composition gradient and visual screening of electrocatalytic activity,

Langmuir 31 (2015) 13238–13246, https://doi.org/10.1021/acs.langmuir.5b02945
[17] P. Mu, Y. Li, Y. Zhang, Y. Yang, R. Hu, X. Zhao, A. Huang, R. Zhang, X.Y. Liu, Q. Huang, C. Lin, High-throughput screening of rat mesenchymal stem cell behavior on gradient TiO_2 nanotubes, ACS Biomater. Sci. Eng. 4 (2018) 2804–2814, https://doi.org/10.1021/acsbiomaterials.8b00488
[18] M. Saqib, J.P. Lai, J.M. Zhao, S.P. Li, G.B. Xu, Bipolar electrochemical approach with a thin layer of supporting electrolyte towards the growth of self-organizing TiO_2 nanotubes, ChemElectroChem 3 (2016) 360–365, https://doi.org/10.1002/celc.201500182
[19] W. Wei, F. Bjorefors, L. Nyholm, Hybrid energy storage devices based on monolithic electrodes containing well-defined TiO_2 nanotube size gradients, Electrochim. Acta 176 (2015) 1393–1402, https://doi.org/10.1016/j.electacta.2015.07.092
[20] G. Loget, S. So, R. Hahn, P. Schmuki, Bipolar anodization enables the fabrication of controlled arrays of TiO_2 nanotube gradients, J. Mater. Chem. A 2 (2014) 17740–17745, https://doi.org/10.1039/c4ta04247f
[21] J. Ni, K. Noh, C.J. Frandsen, S.D. Kong, G. He, T. Tang, S. Jin, Preparation of near micrometer-sized TiO_2 nanotube arrays by high voltage anodization, Mater. Sci. Eng. C 33 (2013) 259–264, https://doi.org/10.1016/j.msec.2012.08.038
[22] Y. Li, S. Wang, Y. Dong, P. Mu, Y. Yang, X. Liu, C. Lin, Q. Huang, Effect of size and crystalline phase of TiO_2 nanotubes on cell behaviors: a high throughput study using gradient TiO_2 nanotubes, Bioact. Mater. 5 (2020) 1062–1070, https://doi.org/10.1016/j.bioactmat.2020.07.005
[23] B. Settles, Active Learning Literature Survey, Mach. Learn. 15 (2010) 201–221, https://doi.org/10.1145/2939672.2939785
[24] D. Cohn, L. Atlas, R.J.M.L. Ladner, Improving generalization with active learning, Mach. Learn. 15 (1996) 201–221, https://doi.org/10.1007/BF00993277
[25] Y. Ruihao, L. Zhen, B.P. V, X. Deqing, Z. Yumei, D. Xiangdong, S. Jun, X. Dezhen, L. Turab, Accelerated discovery of large electrostrains in $BaTiO_3$-based piezoelectrics using active learning, Adv. Mater. 30 (2018) 1702884, https://doi.org/10.1002/adma.201702884
[26] G.X. Gu, C.-T. Chen, D.J. Richmond, M.J. Buehler, Bioinspired hierarchical composite design using machine learning: simulation, additive manufacturing, and experiment, Mater. Horiz. 5 (2018) 939–945, https://doi.org/10.1039/C8MH00653A
[27] R. Razavi, A. Sabaghmoghadam, A. Bemani, A. Baghban, K.-w Chau, E. Salwana, Application of ANFIS and LSSVM strategies for estimating thermal conductivity enhancement of metal and metal oxide based nanofluids, Eng. Appl. Comp. Fluid Mech. 13 (2019) 560–578, https://doi.org/10.1080/19942060.2019.1620130
[28] M.H. Ahmadi, B. Mohseni-Gharyehsafa, M. Farzaneh-Gord, R.D. Jilte, R. Kumar, K.-w Chau, Applicability of connectionist methods to predict dynamic viscosity of silver/water nanofluid by using ANN-MLP, MARS and MPR algorithms, Eng. Appl. Comp. Fluid Mech. 13 (2019) 220–228, https://doi.org/10.1080/19942060.2019.1571442
[29] A. Baghban, A. Jalali, M. Shafiee, M.H. Ahmadi, K.-w Chau, Developing an ANFIS-based swarm concept model for estimating the relative viscosity of nanofluids, Eng. Appl. Comp. Fluid Mech. 13 (2019) 26–39, https://doi.org/10.1080/19942060.2018.1542345
[30] M.-L. Zhang, Z.-H. Zhou, ML-KNN: a lazy learning approach to multi-label learning, Pattern Recognit. 40 (2007) 2038–2048, https://doi.org/10.1016/j.patcog.2006.12.019
[31] A.E. Raftery, T. Gneiting, F. Balabdaoui, M. Polakowski, Using bayesian model averaging to calibrate forecast ensembles, Mon. Weather Rev. 133 (2005) 1155–1174, https://doi.org/10.1175/MWR2906.1
[32] V. Cherkassky, Y. Ma, Practical selection of SVM parameters and noise estimation for SVM regression, Neural Netw. 17 (2004) 113–126, https://doi.org/10.1016/s0893-6080(03)00169-2
[33] F. Li, J. Han, T. Cao, W. Lam, B. Fan, W. Tang, S. Chen, K.L. Fok, L. Li, Design of self-assembly dipeptide hydrogels and machine learning via their chemical features, Proc. Natl. Acad. Sci. 116 (2019) 11259–11264, https://doi.org/10.1073/pnas.1903376116
[34] F. Pedregosa, G. Varoquaux, A. Gramfort, V. Michel, B. Thirion, O. Grisel, M. Blondel, P. Prettenhofer, R. Weiss, V. Dubourg, J. Vanderplas, A. Passos, D. Cournapeau, M. Brucher, M. Perrot, É. Duchesnay, Scikit-learn: machine learning in python, J. Mach. Learn. Res. 12 (2011) 2825–2830 https://jmlr.org/papers/v12/pedregosa11a.html.
[35] J. Reid, M. Sigman, Holistic prediction of enantioselectivity in asymmetric catalysis, Nature 571 (2019) 343–348, https://doi.org/10.1038/s41586-019-1384-z
[36] A. Jagannath, T. Tsuchido, Validation of a polynomial regression model: the thermal inactivation of Bacillus subtilis spores in milk, Lett. Appl. Microbiol. 37 (2003) 399–404, https://doi.org/10.1046/j.1472-765X.2003.01416.x
[37] M. Sahaluddin, I.O. Alade, M.O. Oyedeji, U.Sa Aliyu, A machine learning-based model to estimate the density of nanofluids of nitrides in ethylene glycol, J. Appl. Phys. 127 (2020) 205105, https://doi.org/10.1063/5.0002753
[38] J. Jie, Z. Hu, G. Qian, M. Weng, S. Li, S. Li, M. Hu, D. Chen, W. Xiao, J. Zheng, L.-W. Wang, F. Pan, Discovering unusual structures from exception using big data and machine learning techniques, Sci. Bull. 64 (2019) 612–616, https://doi.org/10.1016/j.scib.2019.04.015
[39] S. Alotaibi, M.A. Amooie, M.H. Ahmadi, N. Nabipour, K.-w Chau, Eng. Appl. Comp. Fluid Mech. 14 (2020) 379–390, https://doi.org/10.1080/19942060.2020.1715843
[40] M. Sadeghzadeh, H. Maddah, M.H. Ahmadi, A. Khadang, M. Ghazvini, A. Mosavi, N. Nabipour, Prediction of thermo-physical properties of TiO_2-Al_2O_3/water nanoparticles by using artificial neural network, Nanomaterials 10 (2020) 697, https://doi.org/10.3390/nano10040697
[41] T. Lookman, P.V. Balachandran, D. Xue, R. Yuan, Active learning in materials science with emphasis on adaptive sampling using uncertainties for targeted design, npj Comput. Mater. 5 (2019) 21, https://doi.org/10.1038/s41524-019-0153-8
[42] F. Han, S. Lv, Z. Li, L. Jin, B. Fan, J. Zhang, R. Zhang, X. Zhang, L. Han, J. Li, Triple-synergistic 2D material-based dual-delivery antibiotic platform, NPG Asia Mater. 12 (2020) 15, https://doi.org/10.1038/s41427-020-0195-x
[43] R. Huang, M. Hu, W. Liang, J. Zheng, Y. Du, Y. Lin, H. Wang, W. Guo, Z. Zeng, C. Li, M. Li, H. Wang, X. Zhang, One-step preparation of green fabric for continuous antibacterial applications, Engineering 7 (2021), https://doi.org/10.1016/j.eng.2020.08.022
[44] S. Chen, S. Zhang, M. Galluzzi, F. Li, X. Zhang, X. Yang, X. Liu, X. Cai, X. Zhu, B. Du, J. Li, P. Huang, Insight into multifunctional polyester fabrics finished by one-step eco-friendly strategy, Chem. Eng. J. 358 (2019) 634–642, https://doi.org/10.1016/j.cej.2018.10.070
[45] J. Ouyang, X. Ji, X. Zhang, C. Feng, Z. Tang, N. Kong, A. Xie, J. Wang, X. Sui, L. Deng, Y. Liu, J.S. Kim, Y. Cao, W. Tao, In situ sprayed NIR-responsive, analgesic black phosphorus-based gel for diabetic ulcer treatment, Proc. Natl. Acad. Sci. U. S. A. 117 (2020) 28667–28677, https://doi.org/10.1073/pnas.2016268117
[46] Y. Du, Z. Huang, S. Wu, K. Xiong, X. Zhang, B. Zheng, R. Nadimicherla, R. Fu, D. Wu, Preparation of versatile yolk-shell nanoparticles with a precious metal yolk and a microporous polymer shell for high-performance catalysts and antibacterial agents, Polymer 137 (2018) 195–200, https://doi.org/10.1016/j.polymer.2017.12.069